Inorganic Chemistry
Article
Cite This: Inorg. Chem. XXXX, XXX, XXX−XXX
pubs.acs.org/IC

Ferrocene-Appended Iridium(III) Complexes: Configuration Regulation, Anticancer Application, and Mechanism Research

Xingxing Ge, Shujiao Chen, Xicheng Liu,* Qinghui Wang, Lijun Gao, Chengfeng Zhao, Lei Zhang, Mingxiao Shao, Xiang-Ai Yuan, Laijin Tian, and Zhe Liu*

Institute of Anticancer Agents Development and Theranostic Application, Key Laboratory of Life-Organic Analysis and Key Laboratory of Pharmaceutical Intermediates and Analysis of Natural Medicine, School of Chemistry and Chemical Engineering, Qufu Normal University, Qufu 273165, China

Supporting Information

ABSTRACT: A series of ferrocene-appended half-sandwiched iridium(III) phenylpyridine complexes have been designed and synthesized. These complexes show better anticancer activity than cisplatin widely used in clinic under the same conditions. Meanwhile, complexes could effectively inhibit cell migration and colony formation. Complexes could interact with protein and transport through serum protein, effectively catalyzing the oxidation of nicotinamide−adenine dinucleotid and inducing the accumulation of reactive oxygen species (ROS, $^1O_2$), which confirmed the anticancer mechanism of oxidation. Furthermore, laser scanning confocal detection indicates that these complexes can enter cells followed by a non-energy-dependent cellular uptake mechanism, effectively accumulating in the lysosome (Pearson's colocalization coefficient: ∼0.90), leading to lysosome damage, and reducing the mitochondrial membrane potential (MMP). Taken together, ferrocene-appended iridium(III) complexes possess the prospect of becoming a new multifunctional therapeutic platform, including lysosome-targeted imaging and anticancer drugs.

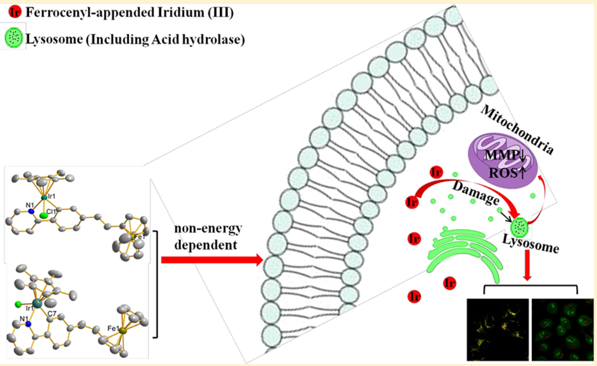

1. INTRODUCTION

Globally, cancer is responsible for one-sixth of the deaths, including 9.6 million in 2018.[1] Although most small organic molecules and biologically derived compounds have been approved for medical treatment and dominate the pharmaceutical market, metallodrugs still attract much attention because of their unique biological and chemical characteristics.[2−4] Cisplatin was the first metalloanticancer therapeutic agent for clinical application and initiated a new field in the application of transition-metal complexes for therapeutic design. However, some undesirable side effects, including high systemic toxicity, drug resistance, low selectivity for the target DNA, and inefficient bioavailability,[4] have greatly limited its application and development, fueling tremendous research effort into the discovery of other transition-metal complexes with therapeutic properties.

Ferrocene or its derivatives, typical organometallic compounds possessing the advantages of mild reversible redox properties, high stability, lipophilicity, and low toxicity, are highly active against several diseases, especially cancer. Studies showed that the oxidation state of the ferrocenyl moiety plays a crucial role in their cytotoxic effects and put forward an oxidation-related mechanism.[5] Ferrocenium could produce reactive oxygen species (ROS, $^1O_2$), which, in turn, induce DNA damage and finally exhibit their cytotoxic activities.[5−7] Additionally, the last one has entered clinical trials.[8] Compared with other metal complexes, the anticancer potential of simple ferrocene derivatives was generally low; however, the incorporation of a ferrocene group into other transition-metal complexes can effectively improve the anticancer activity of ferrocene.[9] Von Poelhsitz et al. attempted to combine nitrosylruthenium complexes with ferrocene and indicated that the ferrocene ligand plays a crucial role on the anticancer activity of these complexes.[10,11] Rajput et al. prepared a series of ferrocenyl compounds containing pyridine ligands and further studied their coordination behavior with platinum, palladium, rhodium, and iridium.[12] In our previous research, a ferrocene molecule was introduced into triphenyltin compounds.[13] All of these studies indicated that, compared with single metal complexes (ferrocene or other transition-metal complexes), heteronuclear metal complexes all displayed more excellent cytotoxic activity against the cancer cell line.

Iridium(III) (Ir^{III}) complexes have recently burgeoned as promising alternatives to platinum-based organometallic anticancer drugs because of their unique anticancer mechanisms, e.g., involvement in cellular redox reactions (catalyze the oxidation of nicotinamide−adenine dinucleotid and induce

Received: July 24, 2019

ACS Publications

DOI: 10.1021/acs.inorgchem.9b02227
Inorg. Chem. XXXX, XXX, XXX−XXX

the accumulation of ROS) and inhibitor of various proteins [vascular endothelial growth factor receptor 3 (VEGF R3), B-cell lymphoma-2 (Bcl-2), etc.].[14,15] Additionally, the rational design of the ligands around iridium has achieved success in the development of anticancer complexes, including the introduction of C^N-chelating ligands instead of N^N-chelating ligands,[15,16] the replacement of smaller counter-anions with larger ones,[17] etc. Most importantly, integration of the anticancer potencies and the favorable targeted fluorescence characteristics of Ir^{III} complexes supplies us with the possibility to construct novel theranostic platforms.[18]

Different from traditional single metal complexes, multinuclear or heteronuclear metal complexes have confirmed potential advantages in the field of anticancer, including better biological activity and different anticancer mechanisms.[19] Given the great potential of ferrocene and Ir^{III} complexes in the field of anticancer, in this paper, ferrocene-modified phenylpyridine was prepared by the classical Wittig reaction, further reacted with the dimer of Ir^{III}, and constructed the iridium−iron heteronuclear anticancer complexes (complexes **1**−**4**, Figure 1). 3-(4,5-Dimethylthiazol-2-yl)-2,5-diphenyltetrazolium bromide (MTT) assay indicates that iridium−iron complexes show better anticancer activity than ferrocene-modified phenylpyridine (**L1** and **L2**) and half-sandwiched iridium(III) phenylpyridine (**5** and **6**) complexes, especially for trans-configuration complexes (**1** and **3**). In addition, we investigated the mechanism of action and evaluated the imaging capabilities of iridium−iron heteronuclear complexes.

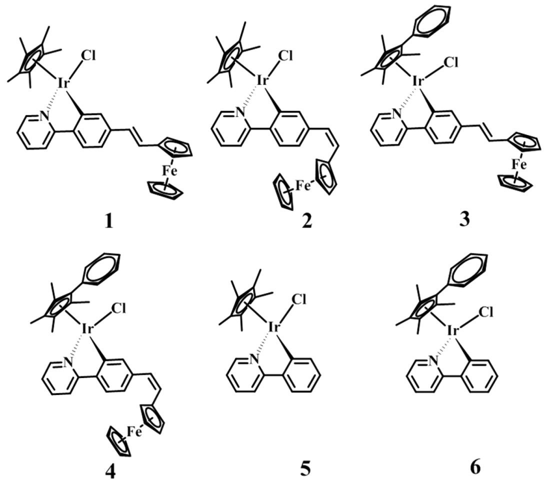

Figure 1. Structures of the designed complexes (**1**−**6**).

2. RESULTS AND DISCUSSION

Ferrocene-appended half-sandwiched Ir^{III} complexes ([(η^5-Cp*)Ir(C^N)Cl]) were obtained by the reaction of [(η^5-C_5Me_5)$IrCl_2$]$_2$ (dimer **1**) and [(η^5-$C_5Me_4C_6H_5$)$IrCl_2$]$_2$ (dimer **2**) with ferrocene-modified phenylpyridine (C^N) ligands (**L1** and **L2**, Scheme 1). C^N-chelating ligands (**L1** and **L2**) were obtained by the classical Wittig reaction, and pure products were obtained by column chromatography.[20] The cis and trans structures were certified by ^{1}H NMR spectroscopy (Figure S1). Hydrogen atoms of the double bonds are shown in the range of 6.0−7.0 ppm with coupling constants of 11.9 and 16.1 Hz, respectively.[21] Complexes **1**−**6** were newly synthesized and obtained in good yields (>80%; Figure 1) and fully characterized by ^{1}H NMR spectroscopy, mass spectrometry (MS), and elemental analysis (Figures S2−S10). Deuterated reagents $CDCl_3$ (7.26 ppm) and $(CD_3)_2SO$ (2.50 ppm) were used as solvents to test the ^{1}H NMR spectra of **1**−**6**. The hydrogen atoms of methylcyclopentadiene (η^5-C_5Me_5) are shown in the range of 1.5−2.0 ppm, and the hydrogen atoms on ferrocene are shown in the range of 4.0−4.5 ppm. Additionally, iridium−iron complexes used multiple solvents in the process of synthesis and purification, including methanol (MeOH; 3.32 ppm) and dichloromethane (5.30 ppm), which showed some residues in the ^{1}H NMR spectra.

Single crystals of complexes **1** and **2** suitable for X-ray diffraction analysis were obtained by the slow diffusion of *n*-hexane into a saturated dichloromethane solution of complexes. The crystal structures of **1** and **2** are depicted in Figure 2A, and crystallographic data are listed in Table S1. Complexes show a "three-leg piano-stool" geometry; interestingly, one crystal unit cell contains two molecules for complex **2**. Obviously, complexes possess the expected *trans*/*cis*-olefin configuration, and ferrocene exhibits the superimposed configuration. The selected bond lengths and angles are shown in Table 1; around the central iridium ion, the distance of Ir−Cl is the longest. This conclusion is consistent with the result that the Ir−Cl bond is the active center of half-sandwiched iridium complexes.[22]

Scheme 1. Synthesis Processes of Ferrocene-Modified Chelating Ligands and Iridium−Iron Complexes

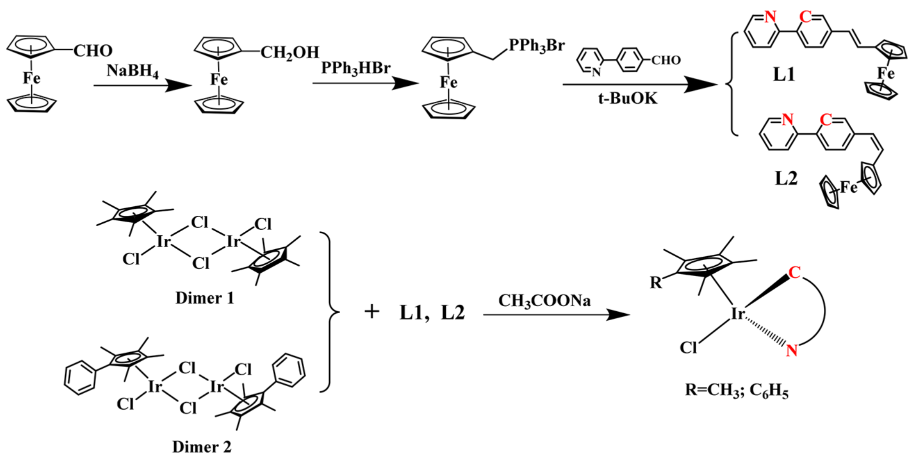

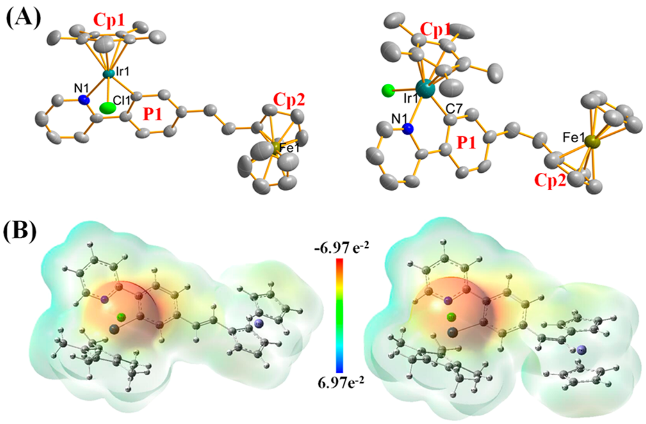

Figure 2. (A) Molecular structures for complexes **1** and **2**. Hydrogen atoms have been omitted for clarity. (B) Color-coded electrostatic potential calculated on the van der Waals surfaces of complexes **1** and **2**.

Table 1. Distances around the Central Iridium and Selected Angles for the Crystals of 1 and 2

	distance (Å)				θ (deg)
complex	Ir−Cp1	Ir−N1	Ir−C7	Ir−Cl1	P1−Cp2
1	1.833	2.101	2.056	2.406	9.39
2	1.830	2.108	2.042	2.417	55.35

2.1. Stability and Electrochemical Properties. The stabilities of complexes **1** and **2** were investigated by ^{1}H NMR spectroscopy at 310 K. Complexes **1** and **2** were dissolved in 80% dimethyl sulfoxide (DMSO)-d_6/20% D_2O (v/v). As shown in Figures S12 and S13, no additional peaks were found in the ^{1}H NMR spectra after 24 h, indicating the stability of iridium−iron complexes under these conditions. In addition, the stability of complexes **1** and **2** was also monitored by UV−vis spectroscopy in a 20% DMSO/80% H_2O (v/v) solution at 298 K for 8 h, and no obvious changes were monitored for the absorbance (Figure S11). Overall, stability studies suggested that these complexes possessed sufficient stability for further studies of the chemical reactivity and biological activity.[23] Cyclic voltammetry (CV) was performed to further investigate the electrochemical properties of complexes **1** and **2** and ferrocene using dichloromethane as the solvent and tetrabutylammonium hexafluorophosphate as the supporting electrolyte (Figures 3 and S21). Complexes **1** and **2** were subjected to two consecutive scans from 0 to 1.3 V at a scan rate of 100 mV s^{-1}. As shown in Figure 3, similar chemical redox behavior, and two reversible redox processes were found to give very strong cathodic peaks at +0.583 and +1.066 V and anodic peaks at +0.259 and +0.754 V for **1** and cathodic peaks at +0.639 and +1.189 V and anodic peaks at +0.242 and +0.804 V for complex **2**. The reversible redox peaks of a1 and a2 correspond to the redox reaction of the ferrocene group, while for the metal iridium, this reaction occurs at b1 and b2. The electrochemical data show that complexes with the analogous structures have similar CV behaviors. A comparison of the cyclic voltammograms of complexes **1** and **2** and ferrocene indicates that ferrocene-modified ligands have no significant effect on the electronic properties of these complexes.

2.2. Cell Cytotoxicity Assay. The anticancer activity of these iron−iridium heteronuclear complexes toward three human cancer cell lines [A549 (lung cancer cells), HeLa (cervical cancer cells), and HepG2 (hepatoma cells)] and the normal cell BEAS-2B (human bronchial epithelioid cells) was determined by MTT assay, and cisplatin was included as a control. The cancer cells were cultivated with different concentrations of complexes for 24 h to obtain the IC_{50} values (the concentration of 50% cell growth is inhibited); unfortunately, no selectivity was observed for cancer cells versus normal cells, and the results are listed in Table 2.

Table 2. IC_{50} Values of Complexes 1−6, Ferrocene-Modified C^N Ligands (L1 and L2), and Cisplatin against A549, Hela, HepG2, and BEAS-2B Cells Determined by MTT Assay after 24 h

	IC_{50} (μM)			
complex	A549	Hela	HepG2	BEAS-2B
1	3.1 ± 0.1	2.4 ± 0.01	2.2 ± 0.01	3.4 ± 0.4
2	5.3 ± 0.1	3.9 ± 0.7	2.4 ± 0.1	3.6 ± 0.1
3	3.2 ± 0.2	3.7 ± 0.4	1.8 ± 0.6	3.3 ± 0.1
4	7.6 ± 0.1	5.3 ± 0.7	3.5 ± 0.3	4.1 ± 0.2
5	27.6 ± 0.6	35.6 ± 1.6	32.3 ± 0.8	
6	8.5 ± 1.4	11.0 ± 0.1	13.6 ± 1.2	
L1	91.9 ± 0.3	10.0 ± 2.0	>100	
L2	72.5 ± 1.6	>100	>100	
cisplatin	21.3 ± 1.7	7.5 ± 0.2	22.7 ± 1.1	

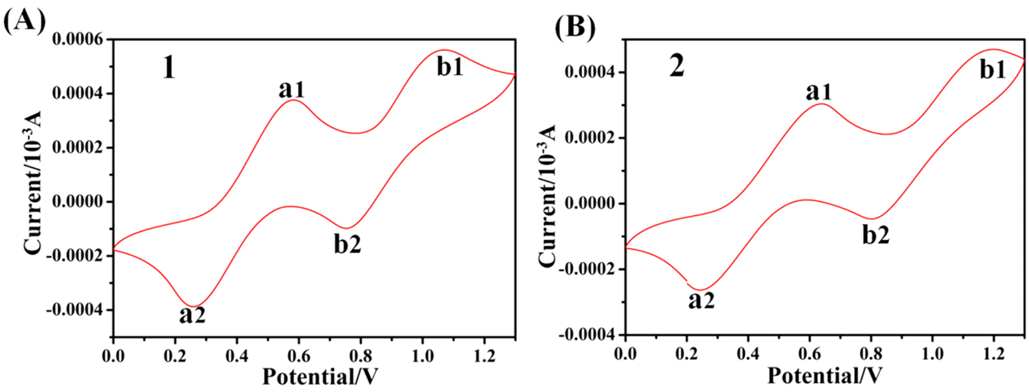

Figure 3. Evaluation of the cyclic voltammograms of **1** and **2** (1 mM) in dichloromethane solutions. Scan rate = 100 mV s^{-1}. Data are quoted as mean ± SD of three replicates.

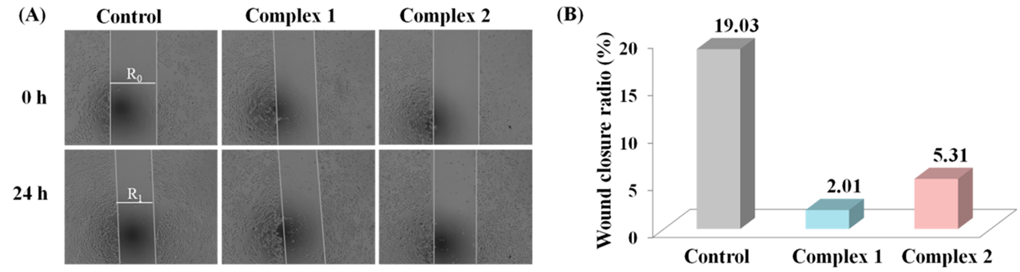

Figure 4. (A) Wound healing assay against A549 cells incubated with complexes **1** and **2** (1.0 × IC_{50}) for 24 h. Scale bar: 200 μM. (B) Histograms of wound healing assay after 24 h. Data are quoted as mean ± SD of three replicates.

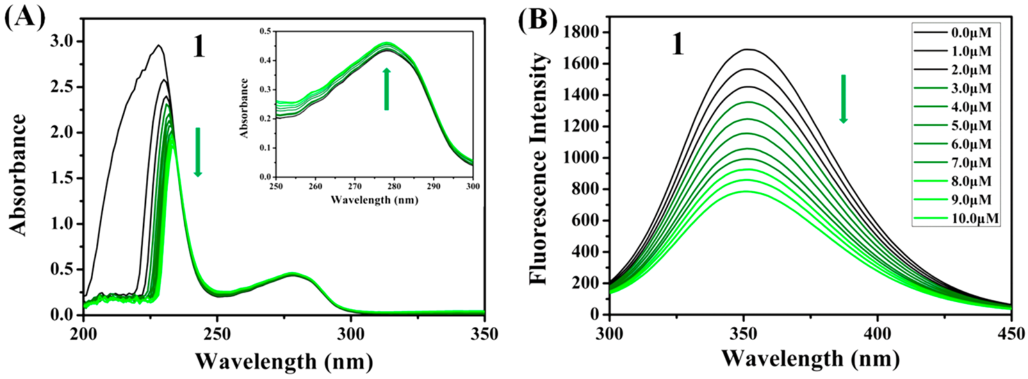

Figure 5. (A) UV−vis spectrum of BSA in a 5 mM Tris-HCl/10 mM NaCl buffer solution (pH = 7.2) with an increase of complex **1** (0−10 μM). The arrows show the direction of changes in absorbance. Inset: Wavelength from 260 to 290 nm. (B) Fluorescence spectra of BSA (5 μM; λ_{ex} = 280 nm; λ_{em} = 350 nm) in the absence and presence of **1** (0−10 μM).

Obviously, these complexes all exhibit consistent sensitivity to A549, Hela, and HepG2 cancer cells. As shown in Table 2, compared with ferrocene-modified C^N ligands (**L1** and **L2**) and ferrocene-unattached structural Ir^{III} complexes **5** ([(η^5-C_5Me_5)Ir(bipy)Cl]PF_6) and **6** ([(η^5-$C_5Me_4C_6H_5$)Ir(bipy)Cl]-PF_6) (Scheme S1), iridium−iron heteronuclear complexes possess better antineoplastic activity under the same conditions and exhibit a certain broad-spectrum characteristic (Figure S22), the best of which (complex **3**) was almost 13 times that of cisplatin (widely used in the clinic) toward HepG2 cells. The results indicate that these heteronuclear complexes possess better anticancer potential after being constructed by the combination of iridium complexes (**5** and **6**) and ferrocene (**L1** and **L2**), which individually show the weaker anticancer activity. Interestingly, the activities of trans-configurational complexes (**1** and **3**) are higher than those of cis-configurational complexes (**2** and **4**), as evidenced by the lower IC_{50} values. To further understand these, quantum chemical computation was used for assessment after comprehensive consideration of the crystal structures of complexes **1** and **2**. The data of natural population analysis (NPA) for the central iridium atom and the leaving group (chlorine) were analyzed by density functional theory calculation at the B3LYP/6-31G(d,p) (C, H, N, Cl)/SDD (Ir) level (Figure 2B). The results of NPA charge population for chlorine in complexes **1** and **2** were almost the same, with values of −0.376 and −0.375; however, those for iridium were 0.078 and 0.093, respectively. This is mainly attributed to the minor dihedral angle (θ) between the **P1** and **Cp2** rings of complex **1** (9.39°), leading to better coplanar property and electron donor capacity for the chelating ligand (**L1**; Table 1). Therefore, the lower the charge of the central iridium ion for complex **1**, the more vulnerable it is to loss of the chlorine ion and the better the anticancer activity.[18,22]

2.3. Inhibition of Migration and Colony Formation.

The metastasis of cancer cells is a complicated process, including digestion of the extracellular matrix, growth of tumors and angiogenesis at new sites, and cell migration to and invasion of the lymphnodes or circulation system.[24−27] Metastasis inhibition is an effective means for cancer treatment. Herein, wound healing assay was performed toward A549 cells to confirm whether iridium−iron complexes might inhibit the migration and invasive properties of tumor cells. As shown in Figure 4, after 24 h of incubation, complexes **1** and **2** (1.0 × IC_{50}) might inhibit cell migration at wound closure ratios [WCR = $(R_0 - R_1)/R_0 \times 100\%$] of 2.01% and 5.31%, respectively. Compared with the vehicle control (19.03%), the smaller WCR indicates that complexes **1** and **2** might inhibit the migration of A549 cells in vitro, and also **1** performs better than **2**, which was consistent with the results of anticancer activity in vitro.

Metastatic cancer cells have to proliferate at new sites to form secondary tumors. Accordingly, for malignant cancer cells, especially for cancer stem cells, colony formation is a crucial feature.[28−30] Complexes **1** and **2** at different concentrations were cultivated to ascertain the inhibition of colony formation. As shown in Figure S23, colony formation can obviously be inhibited after incubation with complexes **1** and **2** at the same concentration (375 and 750 nM). These results showed that complexes could effectively inhibit the growth of cancer cells during a significant period of time.

2.4. Protein Binding Assay.

Human serum albumin (HSA), which can bind a variety of substrates, including metal cations, hormones, and most therapeutic drugs, is the most abundant carrier protein in plasma. Because of the advantages

DOI: 10.1021/acs.inorgchem.9b02227
Inorg. Chem. XXXX, XXX, XXX−XXX

of abundance, ease of purification, stability, medical significance, ligand binding properties, and resemblance to HSA, bovine serum albumin (BSA) was used as a favorable model to study the mechanism of binding.[23,31] In this work, UV−vis absorption and fluorescence spectra were used to investigate the binding of complexes with BSA. As shown in Figures 5A and S14, with an increase of the complexes, a significant reduction of absorption was observed at 227 nm, which is related to the interference between the α-helix of BSA and the complexes. Because of the influence of water (polar solvent), a significant red shift was also found at 218 nm. In addition, a dramatically increase, without any shift at 278 nm, suggested that complexes can interact with BSA and closely relate to the resut that the microenvironment of tryptophan, tyrosine, or phenylalanine (three aromatic acid residues in BSA) was alter. Therefore, to further explore the microenvironment changes in the bonding process, synchronous fluorescence spectra with various concentrations of **1**−**4** were also recorded at the wavelength intervals of $\Delta\lambda$ = 15 and 60 nm, respectively. As shown in Figures S16 and S17, the fluorescence intensities for BSA at 291 and 285 nm ($\Delta\lambda$ = 15 and 60 nm, respectively) were weakened with an increase of the complexes. Additionally, a minor red shift (1−3 nm) occurs at 285 nm ($\Delta\lambda$ = 60 nm) at the investigated concentration range; however, almost no change occurred at the wavelength of $\Delta\lambda$ = 15 nm. The results indicated that the conformation of BSA was changed and the polarity around the tryptophan residues was increased.[32]

In this study, fluorescence spectra were also used to find the nature of complex binding to BSA. As shown in Figures 5B and S15, a significant quenching at 343 nm (the fluorescent emission peak of BSA) was found with an increase of the iridium−iron complexes. The quenching rate constant (K_q) and Stern−Volmer quenching constant (K_{SV}) can be obtained through the classical Stern−Volmer equation, and the binding constant (K_b) and binding site number (n) were calculated through the Scatchard equation (Figures S18 and S19). Fluorescence quenching is usually divided into two different mechanisms: dynamic and static.[33] As shown in Table 3, the values of K_q ranged from 1.25×10^{13} to 2.16×10^{13} M^{-1} s^{-1}, which were almost 1 order of magnitude higher than that of a pure dynamic quenching mechanism ($>2.0 \times 10^{12}$ M^{-1} s^{-1}) and confirmed that iridium−iron complexes could interact with BSA following a static quenching mechanism.[34] Although the values of n ($\approx$1) were almost similar, the K_b values of complexes **1** and **2** are higher than those of complexes **3** and **4**, which indicated that the introduction of too many phenyl groups could increase the steric hindrance between complexes and BSA. For the same reason, complex **1** (trans configuration) shows favorable K_b compared with **2** (cis configuration); similarly, complex **3** > complex **4**. Meanwhile, this conclusion corresponds to the cytotoxicity test in which complexes **1** and **3** show better anticancer activity than the other two complexes.

Table 3. Values of K_{SV}, K_b, K_q, and n for Complexes 1 and 4 at 298 K

complex	K_{SV} ($\times 10^5$ M^{-1})	K_q ($\times 10^{13}$ M^{-1} s^{-1})	K_b ($\times 10^4$ M^{-1})	n
1	1.49 ± 0.11	1.49	8.75	1.18
2	2.16 ± 0.07	2.16	8.20	1.26
3	1.25 ± 0.10	1.25	7.29	1.18
4	1.43 ± 0.10	1.43	1.89	0.87

In summary, the stable combination with BSA suggested that BSA is expected to become an excellent carrier for the delivery of anticancer agents in vivo.

2.5. Catalytic Assay. Being a cofactor, NADH (the reduced state of nicotinamide adenine dinucleotide) plays an important role in regulating energy production in mitochondria. Ruthenium(II), rhodium(III), and iridium(III) complexes have been reported that could catalyze the change of NADH to NAD^+ and induce the production of ROS ($^1O_2$), followed by an anticancer mechanism of oxidation.[35] The interaction between NADH (100 μM) and iridium−iron complexes (1.0 μM) was monitored by UV−vis spectroscopy in 10% MeOH/90% H_2O (v/v) at 298 K after various time intervals. The maximum absorbances of NADH and NAD^+ were monitored at 339 and 259 nm, respectively (Figures 6 and S20). It is evident that the intensity of the absorbance at 339 nm decreased and increased at 259 nm significantly over time. Furthermore, the turnover numbers (TONs), change ratio at 339 nm, were calculated to assess the catalytic efficiency of each complex. The TONs changed from 8.68 to 50.32, especially for complex **1**, indicating the favorable catalytic behavior toward the oxidation of NADH. Additionally, TONs follow the trend **1**, **2** > **3**, **4** and **1** > **2**; **3** > **4**, which contribute to the introduction of a cis-configuration double bond and higher numbers of phenyl, leading to a bigger steric hindrance between the iridium−iron complexes and NADH. Meanwhile, these results were consistent with the conclusions of cellular cytotoxicity and BSA binding.

Excessive ROS accumulation was reported as a major factor causing cell apoptosis.[36,37] In order to investigate the effect of iridium−iron complexes on the production of ROS in cells, the intracellular ROS levels of A549 cells were measured by flow cytometry using an oxidant-sensitive fluorescent probe, dichlorofluorescein−diacetate (DCFH-DA), after treatment with complexes **1** and **2** for 24 h. As shown in Figure S24, the ROS levels showed a dose-dependent increase after treatment with iridium−iron complexes from 0.25 to 0.5 × IC_{50}. Compared with the negative, 2.0 and 1.7 times A549 cells were at high ROS levels for complexes **1** and **2** at the concentration of 0.5 × IC_{50}, respectively. These data were consistent with the catalytic effect of complexes, and excessive production of ROS appears to play a critical role in apoptosis.

2.6. Apoptosis Assay. Apoptosis is a programmed cell death; many transition-metal-based anticancer drugs can inhibit cell growth by activating apoptosis.[38] In this study, cells undergoing apoptosis were identified by flow cytometry with annexin V-FITC/propidium iodide (PI) dual staining after exposure to complexes. As shown in Figure 7 and Tables S4 and S5, complexes induced a dose-dependent increase for apoptotic cells after 24 h. The percentages of late apoptotic cells increased by 78.8% and 53.2% when the concentration changed from 1.0 to 3.0 × IC_{50} for complexes **1** and **2**, respectively. In comparison, 93.7% of the A549 cells survived for the control. This result confirmed that iridium−iron complexes could lead to cell death through a high incidence of apoptosis, which was consistent with the conclusion of MTT assay.

Generally, Ir^{III} complexes exert their anticancer effects and induce function decline through disruption of the cell cycle. To investigate the effect of these complexes on cell cycle arrest, flow cytometry was used to analyze the DNA content of A549 cells stained by PI. The results are shown in Figure 8 and Tables S2 and S3, which were obtained after A549 cells were

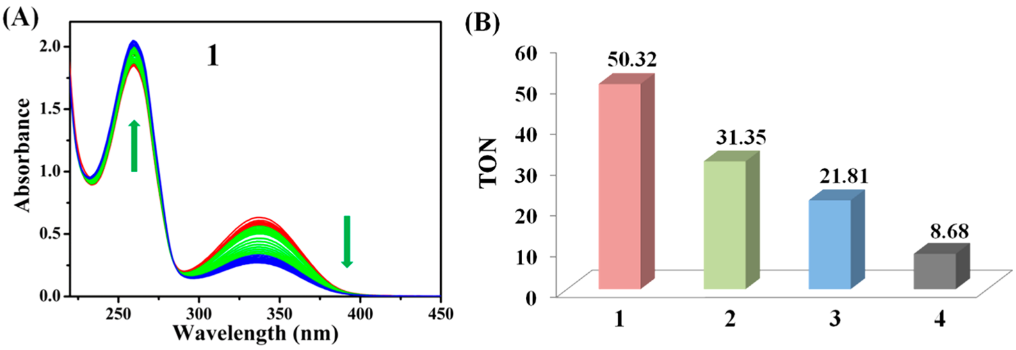

Figure 6. Reaction of complex **1** (1.0 μM) and NADH (100 μM) in a 60% MeOH/40% H_2O (v/v) mixed solution monitored by UV−vis at 298 K over 8 h. (B) TONs of complexes **1**−**4**.

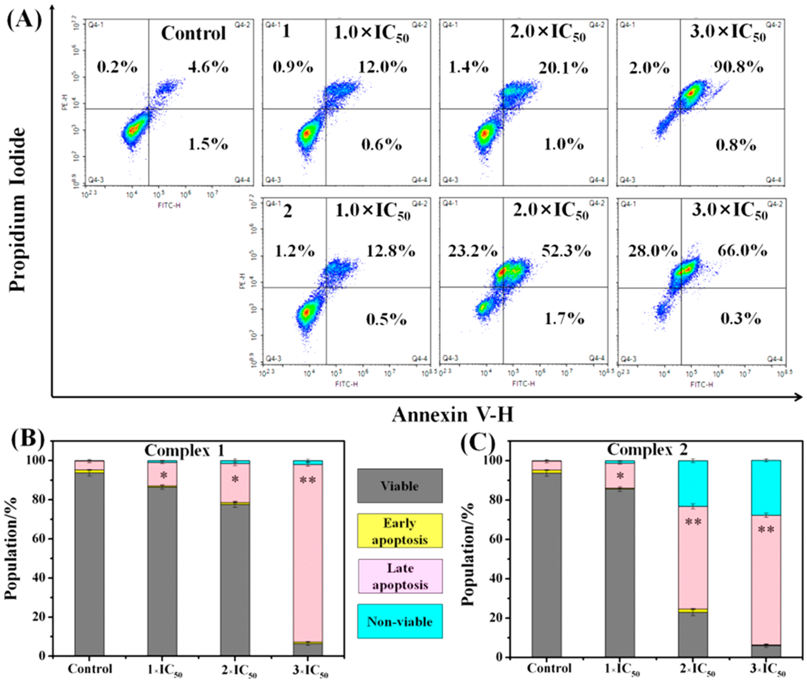

Figure 7. (A) Apoptosis of A549 cells analyzed by flow cytometry after treatment with complexes **1** and **2** (concentrations = 1.0, 2.0, and 3.0 × IC_{50}) and annexin V-FITC/PI stained for 24 h at 310 K. (B) Histograms of four stages for A549 cells induced by complexes **1** and **2**. Data were averaged for three replicate experiments ± SD. *p* values were calculated after a *t* test against the negative control data: *, $p < 0.05$; **, $p < 0.01$.

exposed to complexes **1** and **2** for 24 h at the concentrations of 0.25, 0.5, 1.0, and 2.0 × IC_{50}. As shown, complexes **1** and **2** might induce cell cycle disorder and lead to a dose-dependent increase in the Sub-G1 phase, the population of which increased by 10.03% and 14.85% for complexes **1** and **2** at the concentration of 2.0 × IC_{50}, respectively. The obviously dose-dependent-increased Sub-G1 peak usually correlated with apoptosis,[39] and this conclusion indicated that iridium−iron complexes might induce cell death through regulation of the cell cycle.[40]

Apoptosis is often closely related to the regulation mechanism of mitochondria and accompanied by changes of the mitochondrial membrane potential (MMP); meanwhile, the decrease of MMP is an important signal in the early apoptotic process.[41] To clarify whether complex-induced apoptosis occurred through the destruction of mitochondrial homeostasis, flow cytometry was used to detect the depolarization of MMP with JC-1 (an ideal fluorescent probe for detecting MMP) staining. JC-1-treated cells demonstrate green and red channels on the flow cytometers, and red fluorescence (JC-1 aggregate) can shift to green fluorescence (JC-1 monomer) when MMP declines. As shown in Figure S25 and Tables S6 and S7, a significant dose-dependent decline of MMP occurs in A549 cells induced by complexes **1** and **2** for 24 h, and the population of mitochondrial-membrane-depolarized cells increased by 62.4% and 52.6% for complexes **1** and **2** with a concentration change from 0.25 × IC_{50} to 2.0 × IC_{50}, respectively. The decline of MMP further confirmed that iridium−iron complexes could influence the mitochondria and contribute to apoptosis.

2.7. Cellular Uptake and Localization Assay.

A favorable intracellular uptake mechanism is beneficial to improvement of the anticancer activity for drugs.[42] The cellular uptake mechanism is mainly divided into two types: energy-dependent (including active transport and endocytosis) and non-energy-dependent (including passive transport and free diffusion). In this study, A549 cells were treated with **1** and **2** at 277 and 310 K for 1 h and then treated with chlorocyanochlorophenyl (metabolic inhibitor, 50 μM) and chloroquine (endocytosis modulator, 50 μM) to determine the

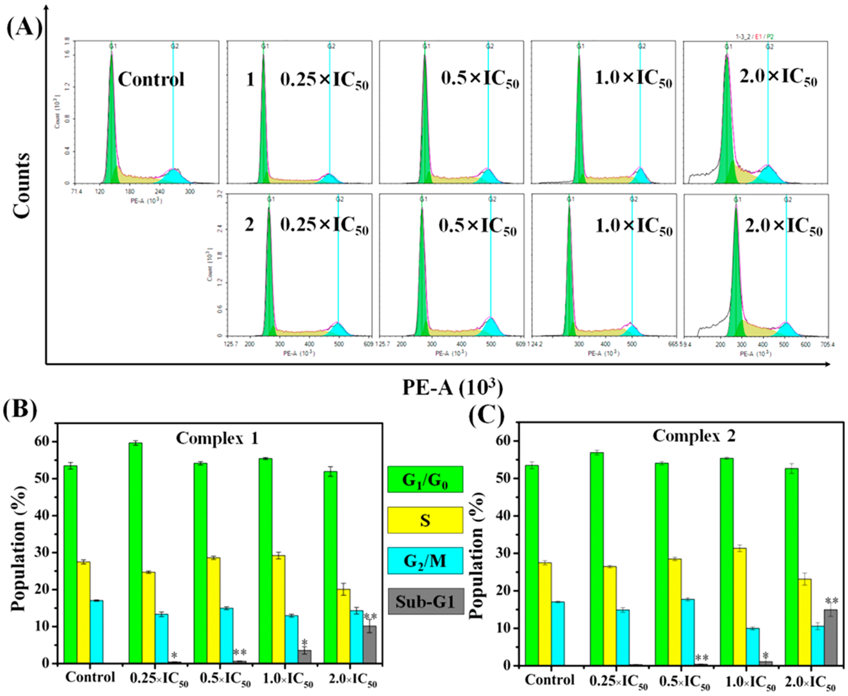

Figure 8. (A) Altered A549 cell cycle analyzed by flow cytometry after being induced by complexes **1** and **2** (concentrations = 0.25, 0.5, 1.0, and 2.0 × IC_{50}) for 24 h at 310 K. (B) Histograms of cell cycle distributions. Data are quoted as mean ± SD of three replicates. p values were calculated after a t test against the negative control data: *, $p < 0.05$; **, $p < 0.01$.

cell uptake mechanisms. As shown in Figures S26 and S27, there were almost no changes compared with the control, which confirmed that the manner in which iridium−iron complexes enter the cells is independent of the endocytosis and energy, therefore, corresponding to cellular uptake of the non-energy-dependent mechanism.[43,44]

Because of the favorable targeted luminescence property of iridium−iron complexes, Lysol Tracker Deep Red (LTDR; lysosome fluorescent probe) and Mito Tracker Deep Red (MTDR; mitochondria fluorescent probe) were used to ascertain the subcellular localization in A549 cells through laser confocal microscopy. As shown in Figure 9, complexes **1** and **2** could effectively accumulate in lysosomes with high Pearson correlation coefficients (PCCs) of 0.90 and 0.91; however, the PCCs of the mitochondria were 0.21 and 0.19, respectively. The results indicated that iridium−iron complexes can enter the cells and accumulate abundantly in lysosomes.

Lysosomes are acidic intracellular organelles (pH = 4.5−5.5) and possess the ability to destroy polysaccharides, proteins, nucleic acids, and other biological macromolecules.[44,45] Once damaged, they release hydrolases, digest the entire cell, and eventually promote apoptosis. Acridine orange (AO), an effective probe (which emits red/green fluorescence in lysosomes/cytosol and nuclei), was utilized to ascertain the integrity of the acidic lysosomes of A549 cells. A549 cells were exposed to complexes **1** and **2** (1.0 × IC_{50} and 3.0 × IC_{50}) for 6 h and then stained with AO (5 μM). As shown in Figure 10, there was a obvious decrease of red fluorescence in the presence of the complexes (1.0 × IC_{50}), and obvious lysosomal damage was found when the concentration of the complexes increased to 3.0 × IC_{50}. The results confirmed that iridium−iron complexes might target lysosomes, lead to lysosomal damage, and eventually induce apoptosis.

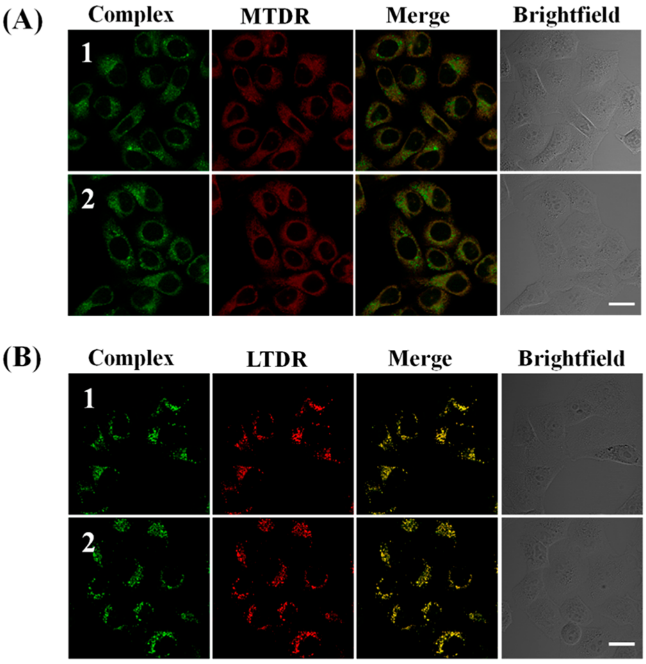

Figure 9. Determination of the intercellular localization of complexes **1** and **2** in A549 cells by confocal microscopy. A549 cells were labeled with MTDR (A) and LTDR (B) and then exposed to **1** and **2** (1.0 × IC_{50}). Complexes **1** and **2** were excited at 488 nm, and the emission was collected at 550 ± 30 nm. MTDR was excited at 644 nm, and the emission was collected at 690 ± 30 nm. LTDR was excited at 594 nm, and the emission was collected at 630 ± 30 nm. Scale bar: 20 μm.

3. CONCLUSION

In this work, four iridium−iron heteronuclear complexes have been designed and synthesized. Iridium−iron complexes show potent anticancer activities toward A549, Hela, and HepG2

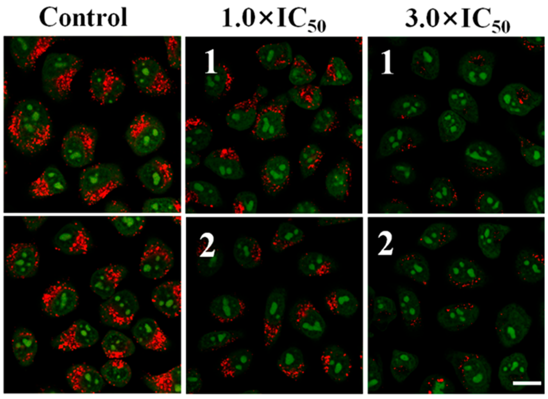

Figure 10. Observation of lysosomal disruption in A549 cells caused by complexes **1** and **2** (1.0 and 3.0 × IC_{50}) with AO (5 μM) staining at 37 °C for 15 min. Emissions were collected at 510 ± 20 nm (green) and 625 ± 20 nm (red) upon excitation at 488 nm. Scale bar: 20 μm.

cells compared with iridium complexes and ferrocene monomers while inhibiting the migration and colony formation of cancer cells. Moreover, these complexes can bind with BSA effectively, show favorable catalytic effects upon a change of the coenzyme NADH to NAD^+, and induce the production of ROS. Laser confocal monitoring indicates that complexes enter the cells in a non-energy-dependent manner, accumulate abundantly in lysosomes, induce damage of the lysosomes, disturb the cell circle, and eventually induce apoptosis. Above all, the combination of ferrocene with iridium(III) complexes may be a promising strategy for the construction of a potential multifunctional heteronuclear metal complex anticancer therapeutic platform.

4. EXPERIMENTAL SECTION

4.1. General Information. $IrCl_3\cdot3H_2O$, phenylpyridine, ferrocenecarboxaldehyde, sodium borohydride, triphenylphosphine hydrobromate, 2-(4-phenylformaldehyde)pyridine, sodium acetate, 2,3,4,5-tetramethyl-2-cyclopentenone (95%), 1,2,3,4,5-pentamethylcyclopentadiene (95%), a *n*-butyllithium solution (1.6 M in hexane), and all kinds of organic solvents [methanol (MeOH), tetrahydrofuran (THF), methylbenzene, etc.] were purchased from Rhea Biotechnology Co. Ltd. For the biological experiments, Dulbecco's modified Eagle medium, fetal bovine serum, a penicillin/streptomycin mixture, and trypsin/ethylenediaminetetraacetic acid were purchased from Sangon Biotech. A549 (lung cancer cells), Hela (cervical cancer cells), and HepG2 (hepatic carcinoma cells) were obtained from Shanghai Institute of Biochemistry and Cell Biology. The appropriate dimers of iridium ($[(\eta^5\text{-}Cp^x)IrCl_2]_2$) were prepared according to literature procedures.[20]

NMR spectra were obtained on Bruker DPX 500 spectrometers, with the chemical shifts reported in parts per million using tetramethylsilane as the internal standard. MS spectra were measured on LCQ Advantage MAX and Bruker MicroTOF QII electrospray ionization (ESI)-quadrupole-time-of-flight (TOF) mass spectrometers. Elemental analysis was performed on a Vario MICRO CHNOS elemental analyzer. UV−vis spectroscopy was performed on a PERSEE TU-1901 UV spectrometer. Fluorescence spectra were collected by a Hitachi F-4600 fluorescence spectrophotometer, with a 400 V voltage and a 5 nm slit width for both excitation and emission. Cyclic voltammogram experiments were carried out using a CH Instrument model 600D electrochemical analyzer/workstation. Induction of apoptosis, cell cycling, and MMP determination were carried out by an ACEA Novocyte 2040R flow cytometry. Viability assay (MTT) was measured using a Perlong DNM-9606 microplate reader at an absorbance of 570 nm. Cell uptake and cellular localization were carried out on a Carl Zeiss AG */LSM/880NLO two-photon laser scanning microscope.

4.2. Synthesis of Ferrocene-Modified Ligands (L1 and L2). **L1** and **L2** were obtained by the classical Wittig reaction:[20,46] Ferrocene Wittig reagents (0.81 g, 1.5 mmol) and 2-(4-phenylformaldehyde)pyridine (0.18 g, 1.0 mmol) were added to a 100 mL round-bottomed flask under nitrogen. Anhydrous THF (40 mL) was added to the above flask and cooled to 0 °C. The THF solution of potassium *tert*-butoxide (0.17 g, 1.5 mmol) was added dropwise to the above flask and stirred for 30 min at 0 °C, followed by stirring at room temperature until 2-(4-phenylformaldehyde)pyridine was consumed completely (monitored by thin-layer chromatography). The reaction was terminated with ice water (80 mL). The resulting precipitate was extracted with THF (30 mL × 3), dried with anhydrous magnesium sulfate, and distilled under reduced pressure. The final product was purified by chromatography on a silica gel column (petroleum ether:ethyl acetate = 15:1 as the eluent), and the data are as follows.

L1. Yield: 0.194 g (53.2%). ^{1}H NMR (500 MHz, $CDCl_3$): δ 8.70 (d, *J* = 4.2 Hz, 1H), 7.99 (d, *J* = 8.2 Hz, 2H), 7.76 (s, 2H), 7.54 (d, *J* = 8.1 Hz, 2H), 7.26 (s, 4H), 6.97 (d, *J* = 16.1 Hz, 1H), 6.74 (d, *J* = 16.1 Hz, 1H), 4.49 (s, 2H), 4.31 (s, 2H), 4.16 (s, 5H).

L2. Yield: 0.189 g (51.8%). ^{1}H NMR (500 MHz, $CDCl_3$): δ 8.70 (d, *J* = 4.7 Hz, 1H), 7.93 (d, *J* = 8.3 Hz, 2H), 7.75 (s, 2H), 7.46 (d, *J* = 8.2 Hz, 2H), 7.24 (d, *J* = 13.8 Hz, 2H), 6.46 (d, *J* = 11.9 Hz, 1H), 6.36 (d, *J* = 11.9 Hz, 1H), 4.22 (s, 2H), 4.16 (s, 2H), 4.11 (s, 5H).

4.3. Synthesis of Iridium−Iron Complexes (1−4). The general synthesis method is as follows: A solution of dimers of iridium (dimer **1**/dimer **2**; 39.8 mg/46 mg, 0.05 mmol), sodium acetate (32.8 mg, 0.4 mmol), and ferrocene-modified phenylpyridine ligands **L** (36.5 mg, 0.1 mmol) in MeOH (40 mL) was stirred at ambient temperature overnight. Most of the solvents were concentrated in vacuum, kept at 253 K for 12 h, filtered, and washed with cold MeOH and diethyl ether. ^{1}H NMR (500 MHz, DMSO-d^6/$CDCl_3$), ESI-MS, matrix-assisted laser desorption/ionization (MALDI)-TOF-MS, and elemental analysis of complexes **1**−**4** are shown in Figures S2, S3, and S6−S9. The data are as follows.

Complex **1**. Yield: 0.063 g (86.5%). ^{1}H NMR (500 MHz, $CDCl_3$): δ 8.67 (d, *J* = 5.4 Hz, 1H), 7.82−7.76 (m, 2H), 7.63 (dd, *J* = 11.2 and 7.6 Hz, 2H), 7.18 (d, *J* = 7.2 Hz, 1H), 7.05 (t, *J* = 6.3 Hz, 1H), 6.93 (d, *J* = 16.0 Hz, 1H), 6.76 (d, *J* = 15.9 Hz, 1H), 4.52 (d, *J* = 24.5 Hz, 2H), 4.31 (s, 2H), 4.18 (s, 5H), 1.71 (s, 15H). MALDI-TOF-MS. Calcd for $C_{33}H_{33}NFeIr$ ($[M - Cl]^+$): *m*/*z* 691.704. Found: *m*/*z* 691.994. Elem anal. Calcd for $C_{33}H_{33}NIrFeCl$: C, 54.51; H, 4.57; N, 1.93. Found: C, 54.78.; H, 4.61; N, 1.90.

Complex **2**. Yield: 0.060 g (82.1%). ^{1}H NMR (500 MHz, $CDCl_3$): δ 8.68 (d, *J* = 5.4 Hz, 1H), 7.77 (d, *J* = 7.8 Hz, 2H), 7.67−7.55 (m, 2H), 7.09−7.02 (m, 2H), 6.50 (d, *J* = 11.8 Hz, 1H), 6.32 (d, *J* = 11.9 Hz, 1H), 4.31 (d, *J* = 58.0 Hz, 2H), 4.16 (d, *J* = 19.7 Hz, 2H), 4.11 (s, 5H), 1.65 (d, *J* = 12.8 Hz, 15H). ESI-MS. Calcd for $C_{33}H_{33}NFeIr$ ($[M - Cl]^+$): *m*/*z* 691.7. Found: *m*/*z* 692.3. Elem anal. Calcd for $C_{33}H_{33}NIrFeCl$: C, 54.51; H, 4.57; N, 1.93. Found: C, 54.75.; H, 4.63; N, 1.86.

Complex **3**. Yield: 0.070 g (88.6%). ^{1}H NMR (500 MHz, $CDCl_3$): δ 8.52 (d, *J* = 5.4 Hz, 1H), 7.78 (d, *J* = 7.2 Hz, 1H), 7.68−7.58 (m, 3H), 7.56−7.49 (m, 2H), 7.44 (d, *J* = 6.2 Hz, 3H), 7.05 (d, *J* = 7.0 Hz, 1H), 6.94 (t, *J* = 6.2 Hz, 1H), 6.60 (d, *J* = 6.2 Hz, 2H), 4.48 (s, 2H), 4.32 (s, 2H), 4.17 (s, 5H), 1.88 (s, 3H), 1.72 (d, *J* = 16.1 Hz, 6H), 1.64 (s, 3H). MALDI-TOF-MS. Calcd for $C_{38}H_{35}NFeIr$ ($[M - Cl]^+$): *m*/*z* 753.770. Found: *m*/*z* 754.044. Elem anal. Calcd for $C_{38}H_{35}NIrFeCl$: C, 57.83; H, 4.47; N, 1.77. Found: C, 58.10.; H, 4.51; N, 1.73.

Complex **4**. Yield: 0.068 g (86.9%). ^{1}H NMR (500 MHz, DMSO): δ 8.46 (d, *J* = 5.5 Hz, 1H), 8.08 (d, *J* = 8.1 Hz, 1H), 7.85−7.78 (m, 2H), 7.48 (s, 1H), 7.32 (d, *J* = 2.8 Hz, 5H), 7.17 (t, *J* = 6.6 Hz, 1H), 6.99 (d, *J* = 8.0 Hz, 1H), 6.38 (d, *J* = 12.0 Hz, 1H), 6.32 (d, *J* = 12.0 Hz, 1H), 4.23 (d, *J* = 32.5 Hz, 2H), 4.17 (s, 2H), 4.10 (s, 5H), 1.71 (s, 3H), 1.61 (d, *J* = 14.6 Hz, 6H), 1.48 (s, 3H). ESI-MS. Calcd for $C_{38}H_{35}NFeIr$ ($[M - Cl]^+$): *m*/*z* 753.8. Found: *m*/*z* 754.3. Elem anal.

Calcd for $C_{38}H_{35}NIrFeCl$: C, 57.83; H, 4.47; N, 1.77. Found: C, 58.04; H, 4.52; N, 1.72.

■ ASSOCIATED CONTENT

Ⓢ Supporting Information

The Supporting Information is available free of charge on the ACS Publications website at DOI: 10.1021/acs.inorgchem.9b02227.

Details of the experimental section, Scheme S1, Figures S1−S27, and Tables S1−S7 (PDF)

Accession Codes

CCDC 1940401 and 1940402 contain the supplementary crystallographic data for this paper. These data can be obtained free of charge via www.ccdc.cam.ac.uk/data_request/cif, or by emailing data_request@ccdc.cam.ac.uk, or by contacting The Cambridge Crystallographic Data Centre, 12 Union Road, Cambridge CB2 1EZ, UK; fax: +44 1223 336033.

■ AUTHOR INFORMATION

Corresponding Authors

*E-mail: chemlxc@163.com (X.L.). Fax: 0086-537-4455228.
*E-mail: liuzheqd@163.com (Z.L.). Fax: 0086-537-4455228.

ORCID

Xicheng Liu: 0000-0002-5932-7206
Zhe Liu: 0000-0001-5796-4335

Notes

The authors declare no competing financial interest.

■ ACKNOWLEDGMENTS

We thank the University Research Development Program of Shandong Province (J18KA082), the National Natural Science Foundation of China (Grants 21671118 and 21703118), the Taishan Scholars Program, Shandong Provincial Natural Science Foundation (Grant ZR2017MB038), and the High Performance Computing Center of Qufu Normal University for support.

■ REFERENCES

(1) World Health Organization, Cancer. http://www.who.int/en/news-room/factsheets/detail/cancer (accessed Sept 28, 2018).

(2) Konkankit, C. C.; Marker, S. C.; Knopf, K. M.; Wilson, J. J. Anticancer activity of complexes of the third row transition metals, rhenium, osmium, and iridium. *Dalton Trans.* **2018**, *47*, 9934−9974.

(3) Zhang, P.; Huang, H. Future potential of osmium complexes as anticancer drug candidates, photosensitizers and organelle-targeted probes. *Dalton Trans.* **2018**, *47*, 14841−14854.

(4) Wang, X.; Wang, X.; Jin, S.; Muhammad, N.; Guo, Z. Stimuli-responsive therapeutic metallodrugs. *Chem. Rev.* **2019**, *119*, 1138−1192.

(5) Osella, D.; Ferrali, M.; Zanello, P.; Laschi, F.; Fontani, M.; Nervi, C.; Cavigiolio, G. On the mechanism of the antitumor activity of ferrocenium derivatives. *Inorg. Chim. Acta* **2000**, *306*, 42−48.

(6) Tabbì, G.; Cassino, C.; Cavigiolio, G.; Colangelo, D.; Ghiglia, A.; Viano, I.; Osella, D. Water stability and cytotoxic activity relationship of a series of ferrocenium derivatives. ESR insights on the radical production during the degradation process. *J. Med. Chem.* **2002**, *45*, 5786−5796.

(7) Kowalski, K.; Hikisz, P.; Szczupak, Ł.; Therrien, B.; Koceva-Chyła, A. Ferrocenyl and dicobalt hexacarbonyl chromones-new organometallics inducing oxidative stress and arresting human cancer cells in G2/M phase. *Eur. J. Med. Chem.* **2014**, *81*, 289−300.

(8) ClinicalTrials.gov Identifier: NCT02497612. https://clinicaltrials.gov/ct2/show/record/NCT02497612 (accessed Sept 28, 2018).

(9) Muenzner, J. K.; Biersack, B.; Albrecht, A.; Rehm, T.; Lacher, U.; Milius, W.; Casini, A.; Zhang, J.; Ott, Ingo.; Brabec, V.; Stuchlikova, O.; Andronache, I. C.; Kaps, L.; Schuppan, D.; Schobert, R. Ferrocenyl-coupled N-heterocyclic carbene complexes of gold(I): A successful approach to multinuclear anticancer drugs. *Chem. - Eur. J.* **2016**, *22*, 18953−18962.

(10) Spencer, J.; Casini, A.; Zava, O.; Rathnam, R. P.; Velhanda, S.; Pfeffer, K. M.; Callear, S. K.; Hursthouse, M. B.; Dyson, P. J. Excellent correlation between cathepsin B inhibition and cytotoxicity for a series of palladacycles. *Dalton Trans.* **2009**, *28*, 10731−10735.

(11) Ornelas, C. Application of ferrocene and its derivatives in cancer research. *New J. Chem.* **2011**, *35*, 1973−1985.

(12) Rajput, J.; Moss, J. R.; Hutton, A. T.; Hendricks, D. T.; Arendse, C. E.; Imrie, C. Synthesis, characterization and cytotoxicity of some palladium(II), platinum(II), rhodium(I) and iridium(I) complexes of ferrocenylpyridine and related ligands. Crystal and molecular structure of trans-dichlorobis(3-ferrocenylpyridine)-palladium(II). *J. Organomet. Chem.* **2004**, *689*, 1553−1568.

(13) Li, J.; Liu, X.; Zhang, H.; Ge, X.; Tang, Y.; Xu, Z.; Tian, L.; Yuan, X.; Mao, X.; Liu, Z. Ferrocenyl−triphenyltin complexes as lysosome-targeted imaging and anticancer agents. *Inorg. Chem.* **2019**, *58*, 1710−1718.

(14) Kastl, A.; Wilbuer, A.; Merkel, A. L.; Feng, L.; Di Fazio, P.; Ocker, M.; Meggers, E. Dual anticancer activity in a single compound: visible-light-induced apoptosis by an antiangiogenic iridium complex. *Chem. Commun.* **2012**, *48*, 1863−1865.

(15) Mou, Z.; Deng, N.; Zhang, F.; Zhang, J.; Cen, J.; Zhang, X. Half-sandwich" Schiff-base Ir(III) complexes as anticancer agents. *Eur. J. Med. Chem.* **2017**, *138*, 72−82.

(16) Liu, Z.; Salassa, L.; Habtemariam, A.; Pizarro, A. M.; Clarkson, G. J.; Sadler, P. J. Contrasting reactivity and cancer cell cytotoxicity of isoelectronic organometallic iridium(III) complexes. *Inorg. Chem.* **2011**, *50*, 5777−5783.

(17) Zhang, H. R.; Guo, L. H.; Tian, Z. Z.; Tian, M.; Zhang, S. M.; Xu, Z. S.; Gong, P. W.; Zheng, X. F.; Zhao, J.; Liu, Z. Significant effects of counteranions on the anticancer activity of iridium(III) complexes. *Chem. Commun.* **2018**, *54*, 4421−4424.

(18) Hao, H. L.; Liu, X. C.; Ge, X. X.; Zhao, Y.; Tian, X.; Ren, T.; Wang, Y.; Zhao, C. F.; Liu, Z. Half-sandwich iridium(III) complexes with α-picolinic acid frameworks and antitumor applications. *J. Inorg. Biochem.* **2019**, *192*, 52−61.

(19) Anderson, C. M.; Jain, S. S.; Silber, L.; Chen, K.; Guha, S.; Zhang, W.; McLaughlin, E. C.; Hu, Y.; Tanski, J. M. Synthesis and characterization of water-soluble, heteronuclear ruthenium(III)/ferrocene complexes and their interactions with biomolecules. *J. Inorg. Biochem.* **2015**, *145*, 41−50.

(20) He, X.; Tian, M.; Liu, X.; Tang, Y.; Shao, C.; Gong, P.; Liu, J.; Zhang, S.; Guo, L.; Liu, Z. Triphenylamine-appended half-sandwich iridium^{III} complexes and their biological applications. *Chem. - Asian J.* **2018**, *13*, 1500−1509.

(21) Liu, Y.; Nishiura, M.; Wang, Y.; Hou, Z. π-conjugated aromatic enynes as a single-emitting component for white electroluminescence. *J. Am. Chem. Soc.* **2006**, *128*, 5592−5593.

(22) Liu, Z.; Romero-Canelón, I.; Qamar, B.; Hearn, J. M.; Habtemariam, A.; Barry, N. P. E.; Pizarro, A. M.; Clarkson, G. J.; Sadler, P. J. The potent oxidant anticancer activity of organoiridium catalysts. *Angew. Chem., Int. Ed.* **2014**, *53*, 3941−3946.

(23) Mukhopadhyay, S.; Gupta, R. K.; Paitandi, R. P.; Rana, N. K.; Sharma, G.; Koch, B.; Rana, L. K.; Hundal, M. S.; Pandey, D. S. Synthesis, structure, DNA/protein binding, and anticancer activity of some half-sandwich cyclometalated Rh(III) and Ir(III) complexes. *Organometallics* **2015**, *34*, 4491−4506.

(24) Dean, Z. S.; Jamilpour, N.; Slepian, M. J.; Wong, P. K. Decreasing wound edge stress enhances leader cell formation during collective smooth muscle cell migration. *ACS Biol. Mater. Sci. Eng.* **2019**, DOI: 10.1021/acsbiomaterials.8b01222.

(25) Liu, T.; Lai, L.; Song, Z.; Chen, T. A sequentially triggered nanosystem for precise drug delivery and simultaneous inhibition of

cancer growth, migration, and invasion. *Adv. Funct. Mater.* **2016**, *26*, 7775−7790.

(26) Liu, M.; Wang, J.; Qi, Q.; Huang, B.; Chen, A.; Li, X.; Wang, J. Nitidine chloride inhibits the malignant behavior of human glioblastoma cells by targeting the PI3K/AKT/mTOR signaling pathway. *Oncol. Rep.* **2016**, *36*, 2160−2168.

(27) Wang, F.; Chen, M.; Lin, Y.; Zhang, H.; Tan, C.; Ji, L.; Mao, Z. Dual functions of cyclometalated iridium(III) complexes: antiMetastasis and lysosome-damaged photodynamic therapy. *ACS Appl. Mater. Interfaces* **2017**, *9*, 42471−42481.

(28) Lei, K. F.; Wu, Z.; Huang, C. Impedimetric quantification of the formation process and the chemosensitivity of cancer cell colonies suspended in 3D environment. *Biosens. Bioelectron.* **2015**, *74*, 878−885.

(29) Tian, Z.; Yang, Y.; Guo, L.; Zhong, G.; Li, J.; Liu, Z. Dual-functional cyclometalated iridium imine NHC complexes: highly potent anticancer and antimetastatic agents. *Inorg. Chem. Front.* **2018**, *5*, 3106−3112.

(30) Wang, F.; Chen, M.; Lin, Y.; Zhang, H.; Tan, C.; Ji, L.; Mao, Z. Dual functions of cyclometalated iridium(III) complexes: antiMetastasis and lysosome-damaged photodynamic therapy. *ACS Appl. Mater. Interfaces* **2017**, *9*, 42471−42481.

(31) Wang, Y.; Wang, X.; Wang, J.; Zhao, Y.; He, W.; Guo, Z. Noncovalent interactions between a trinuclear monofunctional platinum complex and human serum albumin. *Inorg. Chem.* **2011**, *50*, 12661−12668.

(32) Ma, W.; Tian, Z.; Zhang, S.; He, X.; Li, J.; Xia, X.; Chen, X.; Liu, Z. Lysosome targeted drugs: rhodamine B modified N∧N-chelating ligands for half-sandwich iridium(III) anticancer complexes. *Inorg. Chem. Front.* **2018**, *5*, 2587−2597.

(33) Carreira, M.; Calvo-Sanjuán, R.; Sanaú, M.; Zhao, X.; Magliozzo, R. S.; Marzo, I.; Contel, M. Cytotoxic Hydrophilic iminophosphorane coordination compounds of d8 metals. studies of their interactions with DNA and HAS. *J. Inorg. Biochem.* **2012**, *116*, 204−214.

(34) Esteghamat-Panah, R.; Hadadzadeh, H.; Farrokhpour, H.; Mortazavi, M.; Amirghofran, Z. A mononuclear Ru(II) complex with meloxicam: DNA- and BSA-binding, molecular modeling and anticancer activity against human carcinoma cell lines. *Inorg. Chim. Acta* **2017**, *454*, 184−196.

(35) Millett, A. J.; Habtemariam, A.; Romero-Canelon, I.; Clarkson, G. J.; Sadler, P. J. Contrasting anticancer activity of half-sandwich iridium(III) complexes bearing functionally diverse 2-phenylpyridine ligands. *Organometallics* **2015**, *34*, 2683−2694.

(36) Bruce-Keller, A. J.; Begley, J. G.; Fu, W.; Butterfield, D. A.; Bredesen, D. E.; Hutchins, J. B.; Hensley, K.; Mattson, M. P. Bcl-2 protects isolated plasma and mitochondrial membranes against lipid peroxidation induced by hydrogen peroxide and amyloid beta-peptide. *J. Neurochem.* **1998**, *70*, 31−39.

(37) Zhang, Y.; Luo, M.; Zu, Y.; Fu, Y.; Gu, C.; Wang, W.; Yao, L.; Efferth, T. Dryofragin, a phloroglucinol derivative, induces apoptosis in human breast cancer MCF-7 cells through ROS-mediated mitochondrial pathway. *Chem.-Biol. Interact.* **2012**, *199*, 129−136.

(38) Belloc, F.; Belaud-Rotureau, M. A.; Lavignolle, V.; Bascans, E.; Braz-Pereira, E.; Durrieu, F.; Lacombe, F. Flow cytometry detection of caspase 3 activation in preapoptotic leukemic cells. *Cytometry* **2000**, *40*, 151−160.

(39) Li, J.; Tian, M.; Tian, Z.; Zhang, S.; Yan, C.; Shao, C.; Liu, Z. Half-sandwich iridium(III) and ruthenium(II) complexes containing P∧P-chelating ligands: a new class of potent anticancer agents with unusual redox features. *Inorg. Chem.* **2018**, *57*, 1705−1716.

(40) Wang, L.; Li, M.; Cao, P.; Zhang, C.; Huang, F.; Xu, X.; Liu, B.; Zhang, M. Astin B, a cyclic pentapeptide from aster tataricus, induces apoptosis and autophagy in human hepatic L-02 cells. *Chem.-Biol. Interact.* **2014**, *223*, 1−9.

(41) Chen, T.; Liu, Y.; Zheng, W.; Liu, J.; Wong, Y. S. Ruthenium polypyridyl complexes that induce mitochondria-mediated apoptosis in cancer cells. *Inorg. Chem.* **2010**, *49*, 6366−6368.

(42) Qian, C.; Wang, J.; Song, C.; Wang, L.; Ji, L.; Chao, H. The induction of mitochondria-mediated apoptosis in cancer cells by ruthenium(II) asymmetric complexes. *Metallomics* **2013**, *5*, 844−854.

(43) Jin, C.; Liu, J.; Chen, Y.; Li, G.; Guan, R.; Zhang, P.; Ji, L.; Chao, H. Cyclometalated iridium(III) complexes with imidazo[4,5-f][1,10]phenanthroline derivatives for mitochondrial imaging in living cells. *Dalton Trans.* **2015**, *44*, 7538−7547.

(44) Han, Y.; Liu, X.; Tian, Z.; Ge, X.; Li, J.; Gao, M.; Li, Y.; Liu, Y.; Liu, Z. Half-sandwich iridium(III) benzimidazole-appended imidazoliumbased N-heterocyclic carbene complexes and antitumor application. *Chem. - Asian J.* **2018**, *13*, 3697−3705.

(45) Konkankit, C. C.; Marker, S. C.; Knopf, K. M.; Wilson, J. J. Anticancer activity of complexes of the third row transition metals, rhenium, osmium, and iridium. *Dalton Trans.* **2018**, *47*, 9934−9974.

(46) Luzuriaga, L.; Cerdá, M. F. Analysis of the interaction between [Ru (phenanthroline)$_3$]$^{2+}$ and bovine serum albumin. *Adv. Biol. Chem.* **2012**, *2*, 262−267.